Arch. Metall. Mater. **71** (2026), 2, 629-636

DOI: https://doi.org/10.24425/amm.2026.158855

K. PAJOR[1*], M. MAJKA[1], P. BŁYSKUN[2], Ł. GONDEK[3], T. KOZIEŁ[1]

CRYSTALLIZATION BEHAVIOUR OF $Zr_{50}Cu_{40}Al_{10}$ METALLIC GLASS WITH DIFFERENT RELAXED STATE

$Zr_{50}Cu_{40}Al_{10}$ glass-forming alloy was synthesized at different cooling rates conditions, ranging from 10^1 to 10^7 K s^{-1}, to investigate how structural relaxation affects crystallization behaviour and processing stability. XRD confirmed that rapid solidification suppresses crystallization, while DSC revealed supercooled liquid regions. Activation energies obtained by Kissinger and Ozawa analyses increased with cooling rate, reflecting the dominant role of structural disorder induced by high cooling rate delays nucleation via increasing atomic rearrangement cost. These findings clarify the kinetic-thermodynamic balance controlling crystallization and provide guidelines for tailoring Zr-based metallic glasses for thermoplastic forming and controlled nanocrystallization applications

Keywords: Metallic glasses; cooling rate; relaxation; free volume; activation energy of crystallization

1. Introduction

Metallic glasses (MG) are non-crystalline materials obtained via rapid cooling solidification. Avoiding crystallization allows to maintain supercooled liquid phase to glass transition temperature. This random organization of atoms give a number of benefits. Metallic glasses, compared to their crystalline counterparts, are characterized by an isotropy, a high mechanical properties, relatively low Young's modulus with a large elastic deformation, a good corrosion resistance, and other unique physical properties [1]. Such combination of properties dedicate this group of materials for a wide applications, e.g. medicine tools, aerospace, sports equipment, micro and nano-electromechanical systems, luxury goods, and so more. Although the use of metallic glasses is gradually increasing, their full potential has not yet been exploited. The main obstacle to widespread commercialization is the high cost of production associated with the need to use very high purity of both the starting materials and the process itself. So far, many glass-forming systems have been proposed [2], Zr-based bulk metallic glasses attract the most interest due to their combination of properties, glass-forming ability and relatively low cost of raw metals. Even simple binary Zr-Cu system can be vitrify with diameter of 2 mm, that include them in the subgroup of bulk metallic glasses (BMG). The $Zr_{50}Cu_{40}Al_{10}$ alloy is well known in the literature [3-8]. The critical diameter (D_c) can achieve even 16 mm, however, more typical values are between 6 and 8 mm, depending on the purity of starting elements [8,9].

To vitrify liquid, a rapid quenching should be applied to achieve the glass transition temperature (T_g) before crystallization begins. Therefore, the basic parameter describing of glass-forming ability (GFA) is the critical cooling rate (R_c). However, more practical GFA parameters are those based on maximum amorphous thickness (the critical diameter – D_c) or based on the characteristic temperatures (glass transition, crystallization and liquidus) determined in thermal analysis upon heating [2]. Glassy structure is metastable, therefore thermodynamically tends to crystallize, when the crystallization temperature (T_x) is reached. A wider supercooled liquid region ($\Delta T_{xg} = T_x - T_g$) results in the amorphous phase greater stability and resistance to crystallization. Because crystallization is a thermal activated process, some of energy (activation energy, E_c) need to be supplied to overcome the barrier for nucleation and growth of a new phase. This process requires at least reorganization of the nearest atoms and often their distribution over long distances (diffusion). The high stability of the amorphous phase is also associated with a high E_c [10].

The cooling conditions during fabrication strongly influence the glassy state by affecting the atomic structure, free-volume content, and therefore thermal stability and crystallization

[1] AGH UNIVERSITY OF KRAKOW, FACULTY OF METALS ENGINEERING AND INDUSTRIAL COMPUTER SCIENCE, AL. A. MICKIEWICZA 30, 30-059 KRAKOW, POLAND
[2] WARSAW UNIVERSITY OF TECHNOLOGY, FACULTY OF MATERIAL SCIENCE AND ENGINEERING, WOŁOSKA 141, 02-507 WARSAW, POLAND
[3] AGH UNIVERSITY OF KRAKOW, FACULTY OF PHYSICS AND APPLIED COMPUTER SCIENCE, AL. A. MICKIEWICZA 30, 30-059 KRAKOW, POLAND

* Corresponding author: kpajor@agh.edu.pl

kinetics. A higher cooling rate yields a less relaxed structure containing more free volume, which may alter both nucleation and growth of crystals during crystallization [11,12]. It has been demonstrated that structural relaxation strongly influences nucleation kinetics in glasses, as nucleation may evolve concurrently with the relaxation process, leading to an increased nucleation rate [13]. Furthermore, thermal history and enthalpy relaxation have been shown to significantly affect crystallization behaviour in amorphous alloys [14]. In this work, the term "structural relaxation" is used in a relative sense, inferred from differences in cooling rate, rather than directly measured. Although numerous studies have examined the glass-forming ability and thermal behaviour of Zr-based alloys, the direct relationship between the degree of structural relaxation and the activation energy of crystallization in the same alloy system remains not fully clarified.

Therefore, in this work, we investigate the influence of cooling rate (and thus the initial structural state) on the crystallization behaviour of the $Zr_{50}Cu_{40}Al_{10}$ metallic glass. Alloys were produced using different casting techniques to obtain a wide range of cooling rates. The thermal stability, glass transition, and crystallization kinetics were systematically analysed using DSC and correlated with the activation energy of crystallization determined by Kissinger and Ozawa methods.

2. Experimental procedures

The alloy of nominal composition (at.%) $Zr_{50}Cu_{40}Al_{10}$ was prepared using high purity elements of Zr 99,95%, Cu oxygen free high conductivity 99,99%, and Al 99,999%. To obtain a different cooling rates, alloys were cast using two techniques: melt spinning and suction casting with different Water Cooling System Temperature (WCST). The cooling rates for the suction-cast samples (SC3 and SC7) were estimated based on previously reported relationships between cooling rate and cellular spacing measured in a Fe-25%Ni alloy, as described in Ref. [15]. In that study, the influence of mould diameter and cooling conditions on solidification rate was systematically analysed, enabling quantitative estimation of cooling rates in suction casting. For the SC1 sample, the cooling rate was approximated using an empirical relation of the form:

$$CR = 10^{b}\, d^{-a}$$

where d is the casting diameter (mm), and coefficients a and b depend on the WCST (in K), according to:

$$a = 0.0195 \cdot \mathrm{WCST} - 3.6351, \text{ WCST expressed in K}$$

$$b = -0.0059 \cdot \mathrm{WCST} + 4.9746, \text{ WCST expressed in K}$$

The order of magnitude of the cooling rate for the melt spinning process was adopted from literature data reported by Löffler et al. [16], where similar processing conditions yield cooling rates on the order of 10^6 K s^{-1}. All casting parameters and the corresponding estimated cooling rates are summarized in TABLE 1.

Bulk metallic glasses and master alloy for melt spinning were synthesized by means of arc melting (AM, Edmund Bühler GmbH, Germany). Prior to the melting, the chamber was evacuated and flushed with high-purity argon (6N) three times. The ingots were thrice remelted under a Ti-gettered argon atmosphere to obtain composition homogeneity, and then suction cast into a copper moulds cavity. Besides, a ribbon sample was fabricated using the melt spinning method (Melt Spinner HV, Edmund Bühler GmbH, Germany). The copper quenching wheel had a diameter of 250 mm and a linear wheel velocity was set to 30 m s^{-1}.

The phase analysis was conducted by X-ray diffraction with Cu K_α radiation (Malvern Panalytical, The Netherlands) and the diffractograms were analysed using XRD data collected in the 2θ range from 10 to 100°. The microstructure was studied using scanning electron microscopy in the back scattered electrons mode. Atomic composition of the alloys was examined by the energy-dispersive detector (Phenom XL, Thermo Fisher Scientific, U.S.A).

Differential scanning calorimetry (DSC8500, Perkin Elmer, U.S.A) was carried out on thin slices cut from the middle part of the as-cast alloys at a constant heating rate of 20, 40, and 80 K min^{-1} under the protective argon (5N) gas flow of 20 ml min^{-1}. Prior to measurements, the DSC was calibrated by resetting the correction coefficients and performing melting measurements of reference elements (In, Zn, Al) at the applied heating rates. Based on the measured onset melting temperatures and thermal effects, updated correction coefficients were introduced into the software. This calibration procedure ensured a temperature measurement accuracy better than ±1 K. All characteristic temperatures and the crystallization enthalpies were determined by the DSC software. The glass transition temperature T_g was determined at the inflection point of the endothermic heat flow curve corresponding to the glass transition step, using baseline-corrected DSC data according to ASTM E1356 standard. The onset temperature T_x^{onset}, peak temperature T_p, and offset temperature T_x^{offset} of the crystallization event were defined using standard extrapolation methods.

TABLE 1

Parameters of as-cast alloys

Alloy designation	Casting method	As-casts	WCST	Cooling rate
MS	Melt spinning	Ribbon, $d \sim 30$ µm	Room Temperature	~10^6 K s^{-1} [16]
SC1	Suction casting	Plate, $d = 1$ mm	12 ±1°C, 285 K	approx. 2×10^3 K s^{-1} [12]
SC3	Suction casting	Rod, ϕ3 mm	17 ±1°C, 290 K	212 K s^{-1} [12]
SC7	Suction casting	Rod, ϕ7 mm	17 ±1°C, 290 K	39 K s^{-1} [12]

3. Results and discussion

3.1. Structure

The structural analysis was carried out to verify the amorphousness of the obtained alloys and to identify possible crystalline inclusions formed during solidification at different cooling rates. Fig. 1 shows the XRD patterns of samples solidified with different cooling rates. All diffractograms show a broad diffuse halo around 2θ ≈ 30-45°, typical of an amorphous structure, confirming the glassy nature of the rapidly solidified alloys. No distinct crystalline peaks were observed for investigated alloys. Detailed microstructure analysis revealed two types of crystalline areas in SC7 sample (Fig. 2 and TABLE 2). The volume fraction of these phases is below 1%, which explains the absence of detectable diffraction peaks. A large precipitation with a dark contrast is characterized by chemical composition similar to matrix (Spots 3 and 4). Our previous studies shown that equilibrium phases in $Zr_{50}Cu_{40}Al_{10}$ alloy, containing below 200 wt. ppm of oxygen level are $CuZr_2$ and $AlCu_2Zr$ [17]. However, in the case of rapid cooling, polymorphic transformation occurs into the cubic B2 CuZr phase without separation of elements. This phase embedded in a glassy matrix is known undergoes martensitic transformation into the monolithic B19' phase [18-20], which may lead to strain hardening behaviour.

Regular black inclusions (Spots 1 and 2) are characterized by a higher Al and a lower Cu content. Based on EDX results and morphology observations, this phase can be referred to τ_3 with following the chemical composition $Zr_{51}Cu_{28}Al_{21}$ [21]. Such inclusions were observed in many studies and were associated with oxygen contamination [8,9,21-25]. In the BMGs community, this phase is considered as detrimental factor to both glass-forming ability and mechanical properties of Zr-based metallic glasses. It has been shown by Zhou et al. [25], that even small oxygen addition triggers the τ_3 phase formation. In the present study, all suction-cast samples were prepared using the same starting materials and processing procedure, but solidified at different cooling rates. Since the τ_3 phase was observed only in the SC7 sample, this indicates that its formation is primarily influenced by the cooling rate. A sufficiently high cooling rate may effectively suppress the nucleation of this phase [26].

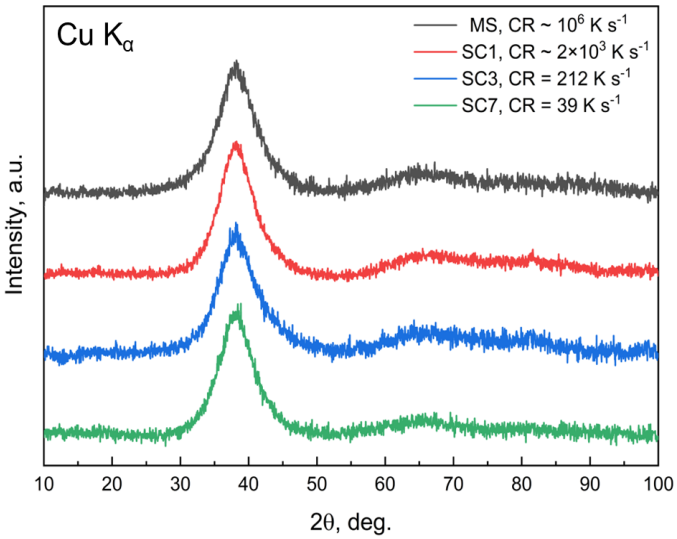

Fig. 1. XRD patterns of $Zr_{50}Cu_{40}Al_{10}$ alloy solidified with various cooling rates (Colour figure online)

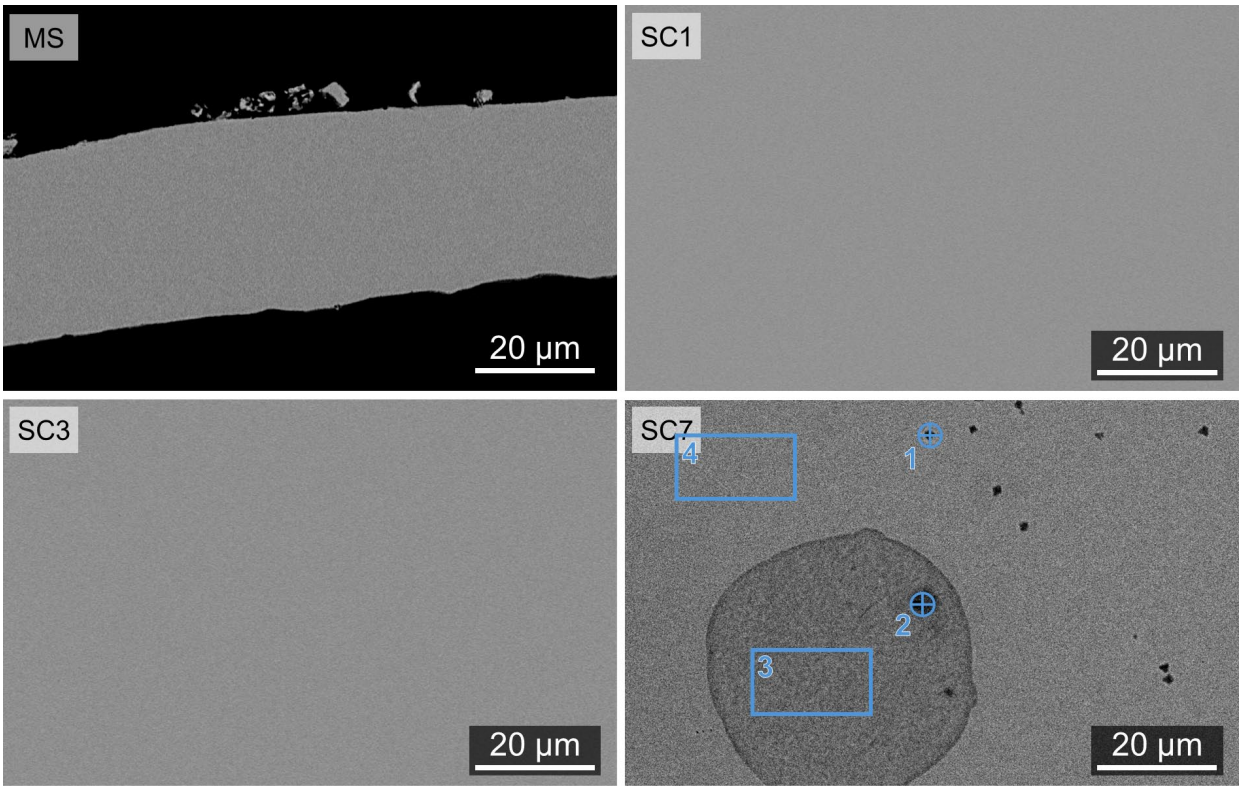

Fig. 2. SEM-BSE image of $Zr_{50}Cu_{40}Al_{10}$ alloy solidified with various cooling rates. EDX spots marked as a blue (Colour figure online)

TABLE 2

Results of SED-EDX semiquantitative analysis of $Zr_{50}Cu_{40}Al_{10}$ alloy suction cast into 7 mm dia. copper mould (Fig. 1)

Spot	Zr	Cu	Al
1	49.7	33.4	16.9
2	49.7	34.2	16.2
3	51.8	37.8	10.4
4	51.7	37.9	10.4

3.2. Calorimetry

Differential scanning calorimetry (DSC) was used to determine the characteristic temperatures, enthalpies of crystallization, and to assess the influence of the cooling rate on the thermal stability of the glassy phase. Fig. 3 shows DSC non-isothermal scanlines. Based on thermograms the characteristic temperatures and enthalpies of crystallization were determined (TABLE 3). The exothermic event (from T_x^{onset} to T_x^{offset}), related to the crystallization, is preceded by a distinct glass transition temperature T_g. An increase in the heating rate (β) shifts all temperatures to higher values, aligning with the thermally activated kinetic transformation process, such as crystallization. As a result, the range of crystallization (ΔT_x) increases from 11-13 K for β = 20 K min^{-1} to 19-21 K for β = 40 K min^{-1} and >27 K for β = 80 K min^{-1}. Those changes also correspond to the increase of the enthalpy of crystallization: about –12 to –13 J g^{-1}, –26 to –28 J g^{-1}, and –57 to –59 J g^{-1} for heating rates of 20, 40, and 80 K min^{-1}, respectively. Generally, in fully glassy samples, increasing the solidification cooling rate causes a slightly lower shifting temperatures.

The variation of T_g with cooling rate was not monotonic. This might have been caused by difficulties in the precise determination of the inflection point at the endothermic hump, especially on curves obtained with heating rate of 80 K min^{-1} heating rate, where disturbance can be noticed. Additionally, deviations from the trends are also present for the SC7 sample, in which partial crystallization was confirmed by SEM observations.

The glass transition temperature uncertain trend translated into the super cooled liquid region behaviour. However, with some caution it can be assumed that decreasing the cooling rate during solidification increased the $T_x^{onset} - T_g$ region. This parameter (ΔT_{xg}) is often used to describe the thermal stability and the resistance of amorphous structure to crystallization [27]. As expected, reducing the cooling rate for the MS, SC1 and SC3 samples increases the thermal stability of the amorphous structure, which is consistent with observations reported by other researchers [7,27,28]. The exception is sample SC7, which

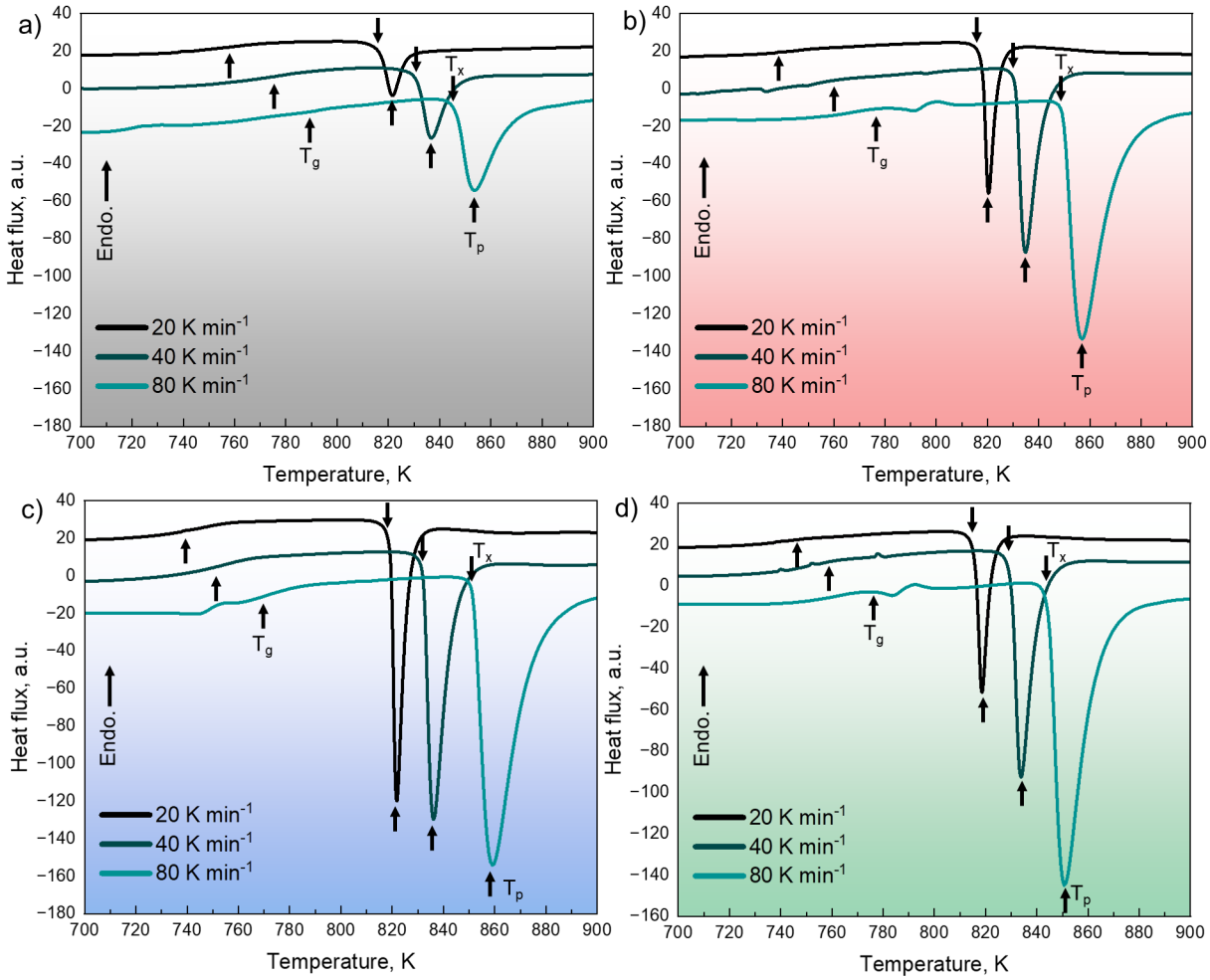

Fig. 3. DSC non-isothermal scans of $Zr_{50}Cu_{40}Al_{10}$ alloy solidified with various cooling rates: a) MS, b) SC1, c) SC3, d) SC7. (Colour figure online)

TABLE 3

The characteristics temperatures from DSC non-isothermal scans (Fig. 2), supercooled liquid region ΔT_{xg}, the range of crystallization event ΔT_x, and enthalpy of crystallization ΔH_x

Alloy	β K min^{-1}	T_g K	T_x^{onset} K	T_p K	T_x^{offset} K	ΔT_{xg} K	ΔT_x K	ΔH_x J g^{-1}
MS	20	758	817	822	828	59	11	–12.43
	40	776	831	837	850	55	19	–26.42
	80	789	846	853	873	57	27	–57.37
SC1	20	743	818	820	828	75	10	–12.41
	40	758	830	835	849	72	19	–28.27
	80	777	850	857	883	73	33	–58.03
SC3	20	740	819	822	832	79	13	–12.96
	40	748	832	836	853	84	21	–27.83
	80	770	852	859	887	82	35	–58.75
SC7	20	745	816	819	827	71	11	–12.36
	40	758	830	834	850	72	20	–26.44
	80	775	845	851	878	70	33	–57.07

exhibits lower stability than SC3, despite an even slower cooling rate. This behaviour is well known in bulk metallic glasses, where even a small volume fraction of crystalline inclusions can significantly reduce the thermal stability of the amorphous matrix by providing heterogeneous nucleation sites [21,29]. In the present case, these deviations can be directly linked to the presence of τ_3 phase inclusions, as confirmed by SEM analysis.

These crystalline regions act as preferential heterogeneous nucleation sites, which facilitates an earlier onset of crystallization and leads to a slight reduction in the thermal stability. Consequently, subtle changes in the characteristic temperatures (particularly T_x^{onset}) and the crystallization enthalpy can be observed compared to fully amorphous samples. Additionally, the presence of τ_3 inclusions may contribute to a broader and less well-defined exothermic peak, reflecting a modified crystallization pathway.

3.3. Activation energy of crystallization

Kissinger approach is widely used for the determination of overall activation energy for crystallization E_p of amorphous state under linear heating conditions [30]. This model is based on the relation between the exothermic peak temperature T_p and the heating rate β through the following equation:

$$\ln\left(\frac{\beta}{T_p^2}\right) = -\frac{E_p}{RT_p} + constant \tag{1}$$

where R is the gas constant (8,314 J mol^{-1} K^{-1}). A plot $\ln(\beta\, T_p^{-2})$ vs. $1000/T_p$ is of linear dependence with a slope of $-E_p/R$. Kissinger plots of $Zr_{50}Cu_{40}Al_{10}$ alloy solidified under different cooling rate are shown in Fig. 4a and calculated activation energies for crystallization E_p are listed in TABLE 4. For all samples without any crystalline areas, increasing the cooling rate caused an increase of the activation energy, meaning that resistance to crystallization is growing with the cooling rate. This observation is opposite to expectations, that a higher cooling rate should lead to less relaxed amorphous structure with more free volume. In such a state atomic mobility should be higher, lowering barrier (activation energy) for crystallization process. To clarify this issue, both kinetic and thermodynamic aspects should be considered. High free volume structure is generally also highly disordered, leading to delay effective nucleation. On the other hand, relaxed glasses are thermodynamically closer to a crystalline phase. This interpretation is consistent with previous studies showing that structural relaxation can enhance nucleation kinetics and modify the crystallization pathway in glasses and amorphous alloys [13,14]. Kissinger method is based on temperature of exothermic event, so it does not differ between nucleation and growth. Plenty of free volume indeed raises diffusivity, but the highly disordered matrix lacks the medium-range order required for efficient crystal embryos; extra atomic rearrangement cost lifts the apparent activation energy. This conclusion is consistent with Louzguine-Luzgin et al. [28], who reported that structural relaxation in Zr-Cu glasses lowers the nucleation barrier. Similar observations were carried out for nanoglasses and high-entropy BMGs: rejuvenation-induced disorder can raise activation energy [31,32].

In alloy cast with the lowest cooling rate (SC7), an activation energy again raised. However, this sample characterized by an occurrence of a trace amount of crystalline phases embedded in the relaxed amorphous matrix, therefore crystallization should be easier (via a heterogenous nucleation mechanism). When crystals are already present, growth becomes diffusion-controlled and the activation barrier increases again due to solute pile-up at the crystal-glass interface [33].

Another approach to activation energy determination is the Ozawa model, given by the following equation [34]:

$$\ln(\beta) = -1.0516\frac{E_p}{RT_p} + constant \tag{2}$$

This formula gives a plot of $\ln(\beta)$ vs. $1000/T_p$ (Fig. 4b and TABLE 4). The activation energies in the peak temperature exhibited a little lower values than in the case of the Kissinger

method, but the trend is the same (Fig. 4c). A similar observation was done by Yuan et al. [35]. To separate nucleation from growth in the crystallization event, a local activation energy need to be calculated. Developing Ozawa's method, isoconversional model (Ozawa-Flynn-Wall, OFW) can be applied [35]:

$$\ln(\beta) = -1.0516\frac{E_c(\alpha)}{RT_\alpha} + constant \tag{3}$$

where T_α corresponds to temperatures at given transformed volume fraction α. Plotting $\ln(\beta)$ vs. $1000/T_\alpha$ allows to obtain a local activation energy at given volume fraction $E_c(\alpha)$. Presenting this data against α shows dynamics of an activation energy through the whole crystallization process (Fig. 4d). The transformation profiles suggests that the energy required for further crystallization decreases as the process progresses. This is consistent with the expectations, therefore as crystallization progress, it becomes easier, indicating a transition from nucleation-controlled to growth-controlled stages. For fully amorphized alloys (MS, SC1 and SC3), the local activation energy is shifted by more or less equal difference along whole process, meaning similar dynamics of transformation. Despite the initial higher barrier in partially crystallized alloy (SC7), steeper decline in E_c can clearly be observed.

According to our previous study [17], the crystallization process may depend on the oxygen content. There [17], the neutron diffraction patterns collected during heating showed a complex crystallization process, even in case of a high purity

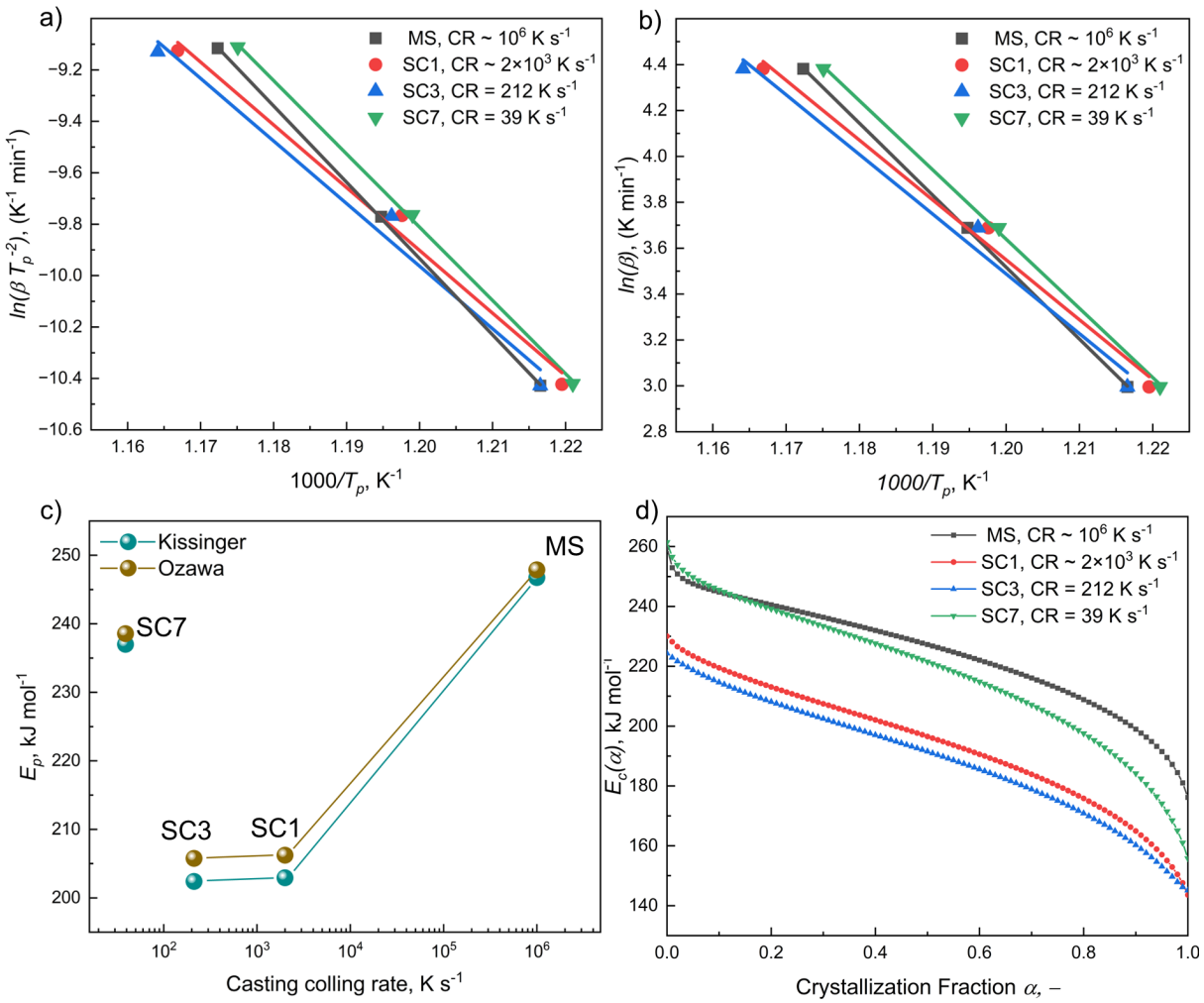

Fig. 4. The activation energies of crystallization: a) Kissinger plots, b) Ozawa plots, c) comparison Kissinger and Ozawa activation energies, d) local activation energy (OFW). (Colour figure online)

TABLE 4

Comparison of Kissinger and Ozawa activation energies of crystallization

Method E_p	MS	R^2	SC1	R^2	SC3	R^2	SC7	R^2
Kissinger, kJ mol^{-1}	246.75	0.9999	202.92	0.9893	202.40	0.9814	236.99	0.9993
Ozawa, kJ mol^{-1}	247.88	0.9999	206.23	0.9838	205.77	0.9906	238.56	0.9994
ΔE_p, kJ mol^{-1}	1.13		3.30		3.36		1.52	

alloy. Initially, $CuZr_2$, $AlCu_2Zr$, and the transition phase appeared together with the amorphous matrix, which later transforms into the B2 CuZr phase. Some researchers assign the transition phase to quasi-crystalline phase [29,36]. In case of partially crystallized alloy, the crystallization process was a little bit wider and more blurry. This showed, that crystals embedded into the amorphous matrix affected the crystallization kinetics of the remaining glassy structure.

4. Conclusions

Understanding the effect of cooling rate on the structural state and crystallization kinetics of Zr-based metallic glasses is crucial for optimizing their processing and stability. In this work, the $Zr_{50}Cu_{40}Al_{10}$ alloy was fabricated using different casting techniques to achieve a wide range of cooling rates, and their thermal stability was analysed through DSC and kinetics modelling. The obtained findings revealed key correlations between structural relaxation, glass-forming ability and activation energies, as summarized below:

1) Fully amorphous structures were obtained for cooling rates above ~200 K s^{-1}, while the sample solidified at a lower rate (~39 K s^{-1}) contained crystalline inclusions.
2) The alloys solidified at higher cooling rates showed higher glass transition (T_g), crystallization onset (T_x), and wider supercooled liquid region (ΔT_{xg}), indicating greater kinetic stability and resistance to crystallization. This confirms that the degree of structural relaxation significantly affects glass stability.
3) The overall activation energy of crystallization, determined using the Kissinger and Ozawa models, increased systematically with the cooling rate. This suggests that more disordered, less relaxed amorphous structures may require higher apparent activation energy due to the additional atomic rearrangements needed for efficient nucleation.
4) Local activation energy ($E_c(\alpha)$) analysis revealed that the energy barrier decreases as crystallization progresses, reflecting the transition from nucleation-controlled to diffusion-controlled growth. The partially crystallized sample (SC7) displayed a higher initial activation barrier, but a more rapid decrease in $E_c(\alpha)$, consistent with heterogeneous nucleation at pre-existing crystalline sites.
5) The obtained results indicate that cooling rate jointly determine both kinetic and thermodynamic aspects of crystallization in Zr-based glasses. Understanding this balance provides valuable guidance for tailoring the thermal stability and processing window of the $Zr_{50}Cu_{40}Al_{10}$ alloys for thermoplastic forming or controlled nanocrystallization applications.

Acknowledgements

This work was financially supported by the Ministry of Science and Higher Education Republic of Poland under contract No. 15.11.110.606.

REFERENCES

[1] A. Inoue, F. Kong, X. Zhu, J. Chen, H. Men, W.J. Botta, Development and industrialization of Zr- and Fe-based bulk metallic glasses and light metal-based metastable alloys. J. Alloys Compd. **979**, 173546 (2024).
DOI: https://doi.org/10.1016/j.jallcom.2024.173546

[2] R. Deng, Z. Long, L. Peng, D. Kuang, B. Ren, A new mathematical expression for the relation between characteristic temperature and glass-forming ability of metallic glasses. J. Non-Cryst. Solids **533**, 119829 (2020).
DOI: https://doi.org/10.1016/j.jnoncrysol.2019.119829

[3] L. Lu, C. Li, W.H. Wang, M.H. Zhu, X.L. Gong, S.N. Luo, Ductile fracture of bulk metallic glass $Zr_{50}Cu_{40}Al_{10}$ under high strain-rate loading. Mater. Sci. Eng. A **651**, 848-853 (2016).
DOI: https://doi.org/10.1016/j.msea.2015.11.040

[4] K.S. Nakayama, Y. Yokoyama, T. Sakurai, A. Inoue, Surface properties of $Zr_{50}Cu_{40}Al_{10}$ bulk metallic glass. Appl. Phys. Lett. **90**, 183105 (2007).
DOI: https://doi.org/10.1063/1.2732168

[5] C.P. Wang, S.B. Tu, Y. Yu, J.J. Han, X.J. Liu, Experimental investigation of phase equilibria in the Zr–Cu–Al system. Intermetallics **31**, 1-8 (2012).
DOI: https://doi.org/10.1016/j.intermet.2012.04.014

[6] S. Zhang, T. Ichitsubo, Y. Yokoyama, K. Miyagi, E. Matsubara, Structural Stability and Elasticity in Zr-Based Bulk Metallic Glasses. Mater. Sci. Forum **561-565**, 1391-1395 (2007).
DOI: https://doi.org/10.4028/www.scientific.net/msf.561-565.1391

[7] S. Zhang, T. Ichitsubo, Y. Yokoyama, T. Yamamoto, E. Matsubara, A. Inoue, Crystallization Behavior and Structural Stability of $Zr_{50}Cu_{40}Al_{10}$ Bulk Metallic Glass. Mater. Trans. **50**, 1340-1345 (2009).
DOI: https://doi.org/10.2320/matertrans.mbw200833

[8] Y. Yokoyama, T. Yamasaki, P.K. Liaw, R.A. Buchanan, A. Inoue, Glass-structure changes in tilt-cast Zr–Cu–Al glassy alloys. Mater. Sci. Eng. A **449-451**, 621-626 (2007).
DOI: https://doi.org/10.1016/j.msea.2006.02.422

[9] K. Pajor, T. Kozieł, G. Cios, P. Błyskun, P. Bała, A. Zielińska-Lipiec, Glass forming ability of the Zr50Cu40Al10 alloy with two oxygen levels. J. Non-Cryst. Solids **496**, 42-47 (2018).
DOI: https://doi.org/10.1016/j.jnoncrysol.2018.05.034

[10] Y. Li, W. Zhang, C. Dong, J. Qiang, A. Makino, Correlation between the glass-forming ability and activation energy of crystallization for $Zr_{75-x}Ni_{25}Al_x$ metallic glasses. Int. J. Miner. Metall. Mater. **20**, 445-449 (2013).
DOI: https://doi.org/10.1007/s12613-013-0749-9

[11] A. Slipenyuk, J. Eckert, Correlation between enthalpy change and free volume reduction during structural relaxation of $Zr_{55}Cu_{30}Al_{10}Ni_5$ metallic glass. Scr. Mater. **50**, 39-44 (2004).
DOI: https://doi.org/10.1016/j.scriptamat.2003.09.038

[12] G. Xing, Q. Hao, F. Zhu, Y.-J. Wang, Y. Yang, H. Kato, E. Pineda, S. Lan, J. Qiao, Correlating dynamic relaxation and viscoelasticity in metallic glasses. Sci. China Phys. Mech. Astron. **67**, 256111 (2024).
DOI: https://doi.org/10.1007/s11433-023-2345-3

[13] V.M. Fokin, A.S. Abyzov, N.S. Yuritsyn, J.W.P. Schmelzer, E.D. Zanotto, Effect of structural relaxation on crystal nucleation in glasses. Acta Materialia **203**, 116472 (2021). DOI: https://doi.org/10.1016/j.actamat.2020.11.014

[14] B. Zang, L. Song, R. Parsons, J. Shen, M. Gao, Y. Zhang, J. Huo, Y. Sun, F. Li, K. Suzuki, J.-Q. Wang, W. Wang, Influence of thermal history on the crystallization behavior of high-Bs Fe-based amorphous alloys. Sci. China Phys. Mech. Astron. **66**, 256111 (2023). DOI: https://doi.org/10.1007/s11433-022-2079-

[15] T. Kozieł, K. Pajor, Ł. Gondek, Cooling rate evaluation during solidification in the suction casting process. J. Mater. Res. Technol. **9**, 13502-13508 (2020). DOI: https://doi.org/10.1016/j.jmrt.2020.09.082

[16] J. Löffler, A.A. Kündig, F.H. Dalla Torre, Rapid Solidification and Bulk Metallic Glasses – Processing and Properties. In: R. Totten (Ed.), Materials Processing Handbook, CRC Press, Boca Raton, (2007).

[17] K. Pajor, B. Rutkowski, Ł. Gondek, P. Błyskun, M. Reehuis, K. Wieczerzak, T. Kozieł, The Scavenging Effect of Different Rare-Earth Elements in the Low-Purity $Zr_{50}Cu_{40}Al_{10}$ Alloy. Metall. Mater. Trans. A **53**, 2902-2925 (2022). DOI: https://doi.org/10.1007/s11661-022-06714-1

[18] T. Kozieł, G. Cios, B. Rutkowski, A. Wierzbicka-Miernik, K. Pajor, P. Bała, Effect of cooling rate during solidification on structure and mechanical properties of $Cu_{45}Zr_{48}A_{17}$ glass-forming alloy. J. Mater. Sci. **58**, 16225-16238 (2023). DOI: https://doi.org/10.1007/s10853-023-09024-y

[19] S. Pauly, G. Liu, G. Wang, U. Kühn, N. Mattern, J. Eckert, Microstructural heterogeneities governing the deformation of $Cu_{47.5}Zr_{47.5}Al_5$ bulk metallic glass composites. Acta Mater. **57**, 5445-5453 (2009). DOI: https://doi.org/10.1016/j.actamat.2009.07.042

[20] F. Jiang, Z.B. Zhang, L. He, J. Sun, H. Zhang, Z.F. Zhang, The effect of primary crystallizing phases on mechanical properties of $Cu_{46}Zr_{47}Al_7$ bulk metallic glass composites. J. Mater. Res. **21**, 2638-2645 (2006). DOI: https://doi.org/10.1557/jmr.2006.0315

[21] Y. Yokoyama, T. Shinohara, K. Fukaura, A. Inoue, Characterization of Crystalline Inclusions in Cast Bulk Zr-Cu-Ni-Al Glassy Alloy. Mater. Trans. **45**, 1819-1823 (2004). DOI: https://doi.org/10.2320/matertrans.45.1819

[22] M.-C. Yeh, P.J. Lo, W.-L. Liu, K.-C. Hsieh, The Microstructure of Zr-Based Bulk Metallic Glass and Glass Matrix Composite. J. Mater. Sci. Eng. B **7**, 135-141 (2017). DOI: https://doi.org/10.17265/2161-6221/2017.7-8.001

[23] Y.F. Xu, L.P.H. Jeurgens, L.C. Lin, S. Ma, S.L. Zhu, Y. Huang, Y.C. Liu, J.W. Qiao, Z.M. Wang, Revealing the univariate effect of structural order on the oxidation of ternary alloys: Amorphous vs. crystalline Cu–Zr–Al alloys. Corros. Sci. **183**, 109309 (2021). DOI: https://doi.org/10.1016/j.corsci.2021.109309

[24] W. Zhang, P. Tao, Y. Chen, J. Si, Z. Long, S. Huang, H. He, Z. Huang, Y. Yang, Structural evolutionary behavior of Zr-based bulk metallic glasses under thermoplastic deformation. Intermetallics **155**.107831 (2023). DOI: https://doi.org/10.1016/j.intermet.2023.107831

[25] W. Zhou, Y. Meng, F. Duan, W. Huang, J. Yao, J. Pan, Y. Wang, Y. Li, The effect of oxygen on phase formation in an industrial Zr based bulk metallic glass. Intermetallics **129**, 107055 (2021). DOI: https://doi.org/10.1016/j.intermet.2020.107055

[26] X.H. Lin, W.L. Johnson, W.K. Rhim, Effect of Oxygen Impurity on Crystallization of an Undercooled Bulk Glass Forming Zr-Ti-Cu-Ni-Al Alloy. Mater. Trans. JIM. **38**, 473-477 (1997). DOI: https://doi.org/10.2320/matertrans1989.38.473

[27] A. Inoue, Stabilization of metallic supercooled liquid and bulk amorphous alloys. Acta Mater. **48**, 279-306 (2000). DOI: https://doi.org/10.1016/S1359-6454(99)00300-6

[28] D.V. Louzguine-Luzgin, I. Seki, T. Wada, A. Inoue, Structural Relaxation, Glass Transition, Viscous Formability, and Crystallization of Zr-Cu–Based Bulk Metallic Glasses on Heating. Metall. Mater. Trans. A **43**, 2642-2648 (2012). DOI: https://doi.org/10.1007/s11661-011-1005-4

[29] J. Eckert, N. Mattern, Crystallization behavior and phase formation in Zr–Al–Cu–Ni metallic glass containing oxygen. Mater. Trans., JIM **39**, 623-632 (1998). DOI: https://doi.org/10.2320/matertrans1989.39.623

[30] S. Vyazovkin, Kissinger Method in Kinetics of Materials: Things to Beware and Be Aware of. Molecules **25**, 2813 (2020). DOI: https://doi.org/10.3390/molecules25122813

[31] J.H. Perepezko, M. Gao, J.-Q. Wang, Nanoglass and Nanocrystallization Reactions in Metallic Glasses. Front. Mater. **8**, 663862 (2021). DOI: https://doi.org/10.3389/fmats.2021.663862

[32] N.H. Nordin, F.S. Mohamad, N.A. Jamal, Non-Isothermal Crystallization Kinetics of a Rapidly Solidified as-Cast TiZrHfNiCu High Entropy Bulk Metallic Glass. World J. Eng. Technol. **8**, 280-295 (2020). DOI: https://doi.org/10.4236/wjet.2020.83023

[33] R.J. Hebert, Nanocrystals in Metallic Glasses. In: Y. Masuda (Ed.), Nanocrystal, IntechOpen, London, (2011).

[34] T. Ozawa, Kinetic analysis of derivative curves in thermal analysis. J. Therm. Anal. **2**, 301-324 (1970). DOI: https://doi.org/10.1007/bf01911411

[35] Z.-Z. Yuan, X.-D. Chen, B.-X. Wang, Y.-J. Wang, Kinetics study on non-isothermal crystallization of the metallic $Co_{43}Fe_{20}Ta_{5.5}B_{31.5}$ glass. J. Alloys Compd. **407**, 163-169 (2006). DOI: https://doi.org/10.1016/j.jallcom.2005.06.022

[36] J.L. Soubeyroux, N. Claret, J.M. Pelletier, Crystallization Behaviour of $Zr_{65-X-Y}Ti_XAl_YHf_5Cu_{20}Ni_{10}$ Bulk Metallic Alloys by in situ Neutron Diffraction. Mater. Sci. Forum **360-362**, 37-42 (2001). DOI: https://doi.org/10.4028/www.scientific.net/msf.360-362.37